

# Geometry Effects on Ignition in Catalytic Monoliths

Karthik Ramanathan and Vemuri Balakotaiah

Dept. of Chemical Engineering, University of Houston, Houston, TX 77204

David H. West

The Dow Chemical Company, Freeport, TX 77541

DOI 10.1002/aic.10120

Published online in Wiley InterScience (www.interscience.wiley.com).

*The convection–diffusion equations with wall reaction are solved for the case of fully developed laminar flow in monoliths having smooth (circular or flat plate) as well as geometries with sharp corners (triangular, rectangular, square, or sinusoidal). The circumferentially averaged Nusselt/Sherwood numbers along the channel length are calculated and their dependency on the local Damköhler number ( $\phi_s^2$ ), solid to fluid conductivity ratio ( $\kappa = k_s/k_f$ ), and monolith aspect ratio ( $d_p/L$ ) is studied. As these parameters are varied, the asymptotic Sherwood/Nusselt numbers are bounded by the constant flux ( $Sh_{H_2}/Nu_{H_2}$ ), the axially constant flux ( $Sh_{H_1}/Nu_{H_1}$ ), and the constant wall temperature ( $Sh_T/Nu_T$ ) asymptotes. For asymmetric geometries, the difference between  $Nu_{H_2}$  and  $Nu_{H_1}$  is a measure of the nonuniformity of ignition in the circumferential direction for  $\kappa = 0$ . When wall conduction is significant ( $\kappa \geq 10$ ), ignition can be predicted accurately by using  $Nu_{H_1}$  value in a one-dimensional model, whereas conversion in the mass transfer controlled regime is determined by  $Sh_T$ . © 2004 American Institute of Chemical Engineers AIChE J, 50: 1493–1509, 2004*

**Keywords:** monolith reactor, catalytic converter, heat transfer coefficient, light-off, ignition

## Introduction

Monolithic catalytic reactors are now used in a number of applications such as emission control, oxidation of VOCs, removal of  $\text{NO}_x$  from exhaust gases, and catalytically stabilized thermal burners. Some advantages of monoliths commonly claimed are low pressure drop compared to packed beds, high geometric surface area, good mass transfer characteristics, and mechanical integrity (no attrition). Catalytic monoliths used in commercial applications have different channel cross sections that include circular, square, triangular, rectangular, sinusoidal, and hexagonal shapes. These

different channel geometries show different ignition behavior because of the asymmetric nature of the geometry, which leads to variation of the heat and mass transfer coefficients in the circumferential direction.

In the study of reactor ignition (light-off) and transient behavior, it is a common practice in the literature to use one-dimensional two-phase models with circumferentially averaged heat and mass transfer coefficients (Heck et al., 1976; Young and Finlayson, 1976). At present, there is no general agreement in the literature on the accuracy of such models compared to the more detailed two- (2-D) and three-dimensional (3-D) models that include transverse variations of the temperature and concentration profiles and conduction in the solid. For example, many studies claim erroneously that 2-D and 3-D models that do not include axial solid conduction (and neglecting axial diffusion) predict a unique steady-state solu-

Correspondence concerning this article should be addressed to V. Balakotaiah at bala@uh.edu.

tion, whereas one-dimensional (1-D) two-phase models predict multiple solutions (Groppi et al., 1995a,b; Heck et al., 1976; Young and Finlayson, 1976).

Likewise, the numerical error that arises in the calculation of Sherwood and Nusselt numbers near ignition/extinction points, attributed to the Gibbs phenomenon, has not been recognized in the literature except for some recent work (Gupta and Balakotaiah, 2001). As shown by Gupta and Balakotaiah (2001) both the 1-D two-phase and the 2-D/3-D models that do not include solid conduction are index infinity differential-algebraic systems and the standard method of solution (discretization in the transverse direction and integration in the axial direction) gives only one of these solutions and even this one solution has significant error near the ignition point, attributed to the Gibbs phenomenon.

Many prior studies have dealt with the determination of heat and mass transfer coefficients in the presence of exothermic reaction in monolith channels of different geometric shapes (Benedetto et al., 2003; Groppi and Tronconi, 1997; Groppi et al., 1995a, 1995b, 2000; Hayes and Kolaczowski, 1994; Hayes et al., 1996; Tronconi and Forzatti, 1992; Young and Finlayson, 1976). Some of these studies focused on channels with a circular cross section, which are axisymmetric and thus do not have the corner effect (Benedetto et al., 2003; Hayes and Kolaczowski, 1994; Hayes et al., 1996). Other studies dealt with circular, triangular, and square channels and focused on finding the average heat and mass transfer coefficients and the variation of these coefficients with the local Damköhler number (Groppi and Tronconi, 1997; Groppi et al., 1995a, 2000; Tronconi and Forzatti, 1992). Groppi et al (1995a) examined the influence of physical property variations, whereas Groppi et al. (2000) investigated the influence of peripheral conduction on the solid temperature profiles. A detailed analysis of how ignition occurs in geometries with corners and the influence of various design and operating parameters on the asymptotic heat and mass transfer coefficients, the light-off boundary, and conversion attained in the ignited (mass transfer controlled) regime is still lacking.

In this work, we determine the variation of the heat and mass transfer coefficients (Nusselt/Sherwood numbers) along the channel perimeter as well as the channel length and the effect of channel geometry, solid conduction, catalyst loading, and channel dimensions on the ignition behavior of the monolith. The fully developed velocity profile is obtained by solving the Navier–Stokes equation and this velocity profile is used in the 3-D convection–diffusion model with wall reaction. The 3-D model is simplified for the case of small and large aspect ratio ( $d_i/L$ ) which gives the Convection and the Short Monolith models corresponding to axial Peclet number of infinity and zero, respectively. These limiting models are used for six different channel geometries to study the ignition behavior and the dependency of the Nusselt/Sherwood numbers on the local Damköhler number as well as other parameters. We also study the influence of geometry on the exit cup-mixing conversion ( $\chi_m$ ). By combining the ignition behavior with the exit conversion in the mass transfer controlled regime, we determine the optimal geometries that facilitate ignition as well as lead to high exit conversion.

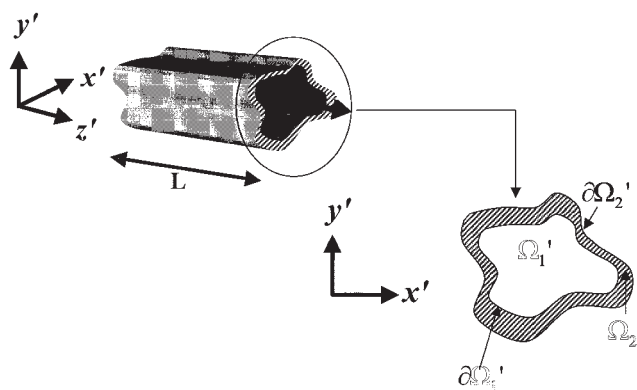


**Figure 1. Diagram and notation used for a monolithic channel of arbitrary shape with finite wall thickness.**

## Mathematical Model

We consider a single channel of a monolith of uniform cross section in which a first-order exothermic wall reaction occurs and assume that the (two-dimensional) velocity field is fully developed. The reaction is assumed to occur on the wall or, in other words, the washcoat is very thin, so diffusional limitations in the washcoat are not important. We also assume that the physical properties (such as density, heat, and mass diffusivities) remain constant. With these assumptions the steady-state concentration and temperature profiles satisfy the following convection–diffusion equations and the boundary conditions (Figure 1)

$$\langle u \rangle \hat{f}(x', y') \frac{\partial C}{\partial z'} = D_m \left( \nabla_*^2 C + \frac{\partial^2 C}{\partial z'^2} \right) \quad (1)$$

$$\rho_f c_p \langle u \rangle \hat{f}(x', y') \frac{\partial T}{\partial z'} = k_f \left( \nabla_*^2 T + \frac{\partial^2 T}{\partial z'^2} \right) \quad (x', y') \in \Omega_1' \quad (2)$$

$$0 = k_s \left( \nabla_*^2 T_s + \frac{\partial^2 T_s}{\partial z'^2} \right) \quad (x', y') \in \Omega_2'; 0 < z' < L \quad (3)$$

$$\langle u \rangle \hat{f}(x', y') C_o = \langle u \rangle \hat{f}(x', y') C - D_m \frac{\partial C}{\partial z'} \quad z' = 0, (x', y') \in \Omega_1' \quad (4)$$

$$\rho_f c_p \langle u \rangle \hat{f}(x', y') T_o = \rho_f c_p \langle u \rangle \hat{f}(x', y') T - k_f \frac{\partial T}{\partial z'} \quad z' = 0, (x', y') \in \Omega_1' \quad (5)$$

$$\frac{\partial C}{\partial z'} = \frac{\partial T}{\partial z'} = 0 \quad z' = L, (x', y') \in \Omega_1' \quad (6)$$

$$\frac{\partial T_s}{\partial z'} = 0 \quad z' = 0, L, (x', y') \in \Omega_2' \quad (7)$$

$$-D_m \nabla_* C \cdot \mathbf{n} = k_w(T_o) C \exp(E/R_g T_o - E/R_g T) \quad \text{on } \partial\Omega'_1, 0 < z' < L \quad (8)$$

$$T_s = T \quad \text{on } \partial\Omega'_1, 0 < z' < L \quad (9)$$

$$k_f \nabla_* T \cdot \mathbf{n} - k_s \nabla_* T_s \cdot \mathbf{n} = (-\Delta H_R) k_w(T_o) C \exp\left(\frac{E}{R_g T_o} - \frac{E}{R_g T}\right) \quad \text{on } \partial\Omega'_1, 0 < z' < L \quad (10)$$

$$\nabla_* T_s \cdot \mathbf{m} = 0 \quad \text{on } \partial\Omega'_2, 0 < z' < L \quad (11)$$

where  $C$  and  $T$  represent the concentration and temperature in the fluid phase,  $\langle u \rangle$  is the average velocity in the channel,  $\Omega'_1$  denotes the channel cross section open to flow,  $\partial\Omega'_1$  is the boundary of  $\Omega'_1$ ,  $x'$  and  $y'$  are the (transverse) coordinates in  $\Omega'_1$ ,  $\nabla_*^2$  is the Laplacian in  $\Omega'_1$ ,  $\langle u \rangle \hat{f}(x', y')$  is the local velocity,  $D_m$  is the diffusivity of the reacting species,  $k_f$  is the thermal conductivity of the gas mixture, and  $T_o$  and  $C_o$  are the inlet temperature and reactant concentration, respectively (for simplicity  $T_o$  and  $C_o$  are assumed to be constant). The heat of the reaction is  $(\Delta H_R)$ ,  $k_w(T_o)$  is the surface reaction rate constant, and  $\mathbf{n}$  is the unit outward normal to  $\partial\Omega'_1$ .  $T_s$  is the temperature in the solid (wall) and  $\Omega'_2$  denotes the wall cross section,  $\partial\Omega'_2$  is the outer boundary of  $\Omega'_2$ ,  $\mathbf{m}$  is the outward normal to  $\partial\Omega'_2$ , and  $k_s$  is the thermal conductivity of the solid. The domain  $\Omega'_1$  is assumed to be simply connected, whereas  $\Omega'_2$  is doubly connected (Figure 1).

The above set of equations can be written in dimensionless form by defining the following set of dimensionless variables and parameters

$$z = \frac{z'}{L} \quad x = \frac{x'}{R_\Omega} \quad y = \frac{y'}{R_\Omega} \quad c = \frac{C}{C_o} \quad f(x, y) = \hat{f}(xR_\Omega, yR_\Omega)$$

$$\theta = \gamma \left( \frac{T - T_o}{T_o} \right) \quad \theta_s = \gamma \left( \frac{T_s - T_o}{T_o} \right) \quad \text{Pe} = \frac{\langle u \rangle L}{D_m} \quad P = \frac{\langle u \rangle R_\Omega^2}{LD_m}$$

$$B = \gamma \frac{(-\Delta H_R) C_o}{\rho_f c_{pf} T_o} \quad \phi_s^2 = \frac{R_\Omega k_w(T_o)}{D_m} \quad \text{Le}_f = \frac{k_f}{\rho_f c_{pf} D_m} \quad \gamma = \frac{E}{R_g T_o}$$

$$\kappa = \frac{k_s}{k_f} \quad \delta_w = \frac{A_{\Omega'_2}}{P_{\Omega'_1}} \quad \delta = \frac{\delta_w}{R_\Omega} \quad \text{Da} = \frac{\phi_s^2}{P} = \frac{Lk_w(T_o)}{\langle u \rangle R_\Omega} \quad (12)$$

where  $R_\Omega$  is the effective transverse diffusion length and is defined as the ratio of the cross-sectional area to the perimeter of the channel ( $R_\Omega = A_{\Omega'_1}/P_{\Omega'_1}$ ). The hydraulic diameter ( $d_h$ )

can be related to the effective transverse diffusion length ( $R_\Omega$ ) by

$$d_h = 4R_\Omega$$

and the aspect ratio ( $\alpha$ ) is defined as the ratio of the hydraulic diameter of the channel to the length of the channel and is given by

$$\alpha = \frac{d_h}{L} = \frac{4R_\Omega}{L}$$

The parameter  $\kappa$  is the ratio of solid to fluid conductivities,  $\delta_w$  is the effective wall thickness, whereas  $\delta$  is the dimensionless wall thickness. In the above set of dimensionless numbers,  $\phi_s^2$  is the square of the transverse Thiele modulus (also referred to as the local Damköhler number) and is equal to the ratio of radial diffusion time to the wall reaction time; the axial Peclet number (Pe) is the ratio of axial diffusion time to convection time and the transverse Peclet number ( $P$ ), is the ratio of radial diffusion time to convection time. The parameter  $B$  is the dimensionless adiabatic temperature increase,  $\gamma$  is the dimensionless activation energy and the fluid Lewis number ( $\text{Le}_f$ ) is the ratio of heat to mass diffusivities. The dimensionless model equations are given by

$$f(x, y) \frac{\partial c}{\partial z} = \frac{1}{P} \nabla^2 c + \frac{1}{\text{Pe}} \frac{\partial^2 c}{\partial z^2} \quad (13)$$

$$f(x, y) \frac{\partial \theta}{\partial z} = \frac{\text{Le}_f}{P} \nabla^2 \theta + \frac{\text{Le}_f}{\text{Pe}} \frac{\partial^2 \theta}{\partial z^2} \quad \text{in } \Omega_1 \quad (14)$$

$$0 = \left( \nabla^2 \theta_s + \frac{\partial^2 \theta_s}{\partial z^2} \right) \quad \text{in } \Omega_2 \quad (15)$$

with the boundary conditions given by

$$\frac{1}{\text{Pe}} \frac{\partial c}{\partial z} = f(x, y)(c - 1) \quad z = 0 \quad (16)$$

$$\frac{\text{Le}_f}{\text{Pe}} \frac{\partial \theta}{\partial z} = f(x, y)\theta \quad z = 0 \quad (17)$$

$$\frac{\partial c}{\partial z} = \frac{\partial \theta}{\partial z} = 0 \quad z = 1 \quad (18)$$

$$\frac{\partial \theta_s}{\partial z} = 0 \quad z = 0 \text{ and } 1 \quad (19)$$

$$-\nabla c \cdot \mathbf{n} = \phi_s^2 c \exp\left(\frac{\theta}{1 + \theta/\gamma}\right) \quad \text{on } \partial\Omega_1, 0 < z < 1 \quad (20)$$

$$\nabla \theta \cdot \mathbf{n} - \kappa \nabla \theta_s \cdot \mathbf{n} = \frac{B\phi_s^2}{\text{Le}_f} c \exp\left(\frac{\theta}{1 + \theta/\gamma}\right) \quad \text{on } \partial\Omega_1, 0 < z < 1 \quad (21)$$

$$\nabla \theta_s \cdot \mathbf{m} = 0 \quad \text{on } \partial\Omega_2, 0 < z < 1 \quad (22)$$

[Note: Here  $\Omega_1$ ,  $\Omega_2$  are scaled domains. The dimensionless wall thickness ( $\delta$ ) enters the model indirectly through Eqs. 15 and 22.] The function  $f(x, y)$  is used to represent the local flow conditions inside the channel. For the case of flat velocity profile  $f(x, y) = 1$ , whereas when we have fully developed laminar flow, the Navier–Stokes equation is solved to get the velocity profile. The Navier–Stokes (in dimensionless form) can be simplified for the case of fully developed unidirectional flow in a channel to

$$\nabla^2 w = -1 \quad \text{in } \Omega_1 \quad (23a)$$

$$w = 0 \quad \text{on } \partial\Omega_1 \quad (23b)$$

where  $w(x, y)$  is the velocity profile (not normalized). The function  $f(x, y)$ , which represents the dimensionless local velocity, is defined as follows:

$$f(x, y) = \frac{w}{\langle w \rangle} \quad (23c)$$

$$\langle w \rangle = \frac{1}{A_{\Omega_1}} \int_{A_{\Omega_1}} w(x, y) dA \quad (23d)$$

For any geometry, the Navier–Stokes equation (Eqs. 23a and 23b) can be solved to obtain  $w$ , which can be used to obtain  $f(x, y)$ . For circular geometry, the function  $f(x, y)$  for fully developed laminar flow is given by  $f(x, y) = 2\{[1 - (x^2 + y^2)]/4\} = 2[(1 - r^2)/4]$  for  $R_{\Omega} = 1$  (and  $0 < r < 2$ ). [Remark: For triangular, rectangular, and square ducts  $f(x, y)$  can be determined analytically.]

We now discuss the two limiting forms of the above model for the case of  $\alpha \rightarrow 0$  (very small aspect ratio or equivalently, axial Peclet number  $Pe \rightarrow \infty$ ) and  $\alpha \rightarrow \infty$  (very large aspect ratio or equivalently,  $Pe \rightarrow 0$ ), which are simpler to understand. The first case, which has been analyzed in previous literature for some geometries, corresponds to the case of an infinitely long tube (the classical Graetz problem with a wall reaction), whereas the second case ( $\alpha \rightarrow \infty$ ) corresponds to a very short monolith. It should be noted that both the limiting cases represent practical situations of a long monolith reactor ( $\alpha \rightarrow 0$ ) and catalytic gauze reactors ( $\alpha \rightarrow \infty$ ), respectively.

### The Short Monolith Model

When the characteristic time for longitudinal diffusion ( $L^2/D_m$ ) is much smaller compared to that for transverse diffusion ( $R_{\Omega}^2/D_m$ ), convection ( $L/\langle u \rangle$ ), and reaction ( $R_{\Omega}/k_w$ ), we can ignore the axial gradients within the monolith and simplify the model by integrating in the axial direction. We assume  $\bar{c} = \bar{c}(x, y) = \int_0^1 c(x, y, z) dz$ , and  $\bar{\theta} = \bar{\theta}(x, y) = \int_0^1 \theta(x, y, z) dz$  and integrate the 3-D model from  $z = 0$  to 1 and substitute the boundary conditions to obtain

$$f(x, y)c(x, y, 1) = \frac{1}{P} \nabla^2 \bar{c} + f(x, y) \quad \text{in } \Omega_1$$

$$f(x, y)\theta(x, y, 1) = \frac{Le_f}{P} \nabla^2 \bar{\theta} \quad \text{in } \Omega_1$$

$$0 = \nabla^2 \bar{\theta}_s \quad \text{in } \Omega_2$$

Given that axial gradients within the monolith are assumed to be small, we use the approximations

$$c(x, y, 1) \approx \bar{c}(x, y) \quad \theta(x, y, 1) \approx \bar{\theta}(x, y)$$

to obtain the model equations

$$f(x, y)(\bar{c} - 1) = \frac{1}{P} \nabla^2 \bar{c} \quad \text{in } \Omega_1 \quad (24)$$

$$f(x, y)\bar{\theta} = \frac{Le_f}{P} \nabla^2 \bar{\theta} \quad \text{in } \Omega_1 \quad (25)$$

$$0 = \nabla^2 \bar{\theta}_s \quad \text{in } \Omega_2 \quad (26)$$

and the boundary conditions

$$-\nabla \bar{c} \cdot \mathbf{n} = \phi_s^2 \bar{c} \exp\left(\frac{\bar{\theta}}{1 + \bar{\theta}/\gamma}\right) \quad \text{on } \partial\Omega_1 \quad (27)$$

$$\nabla \bar{\theta} \cdot \mathbf{n} - \frac{k_s}{k_f} \nabla \bar{\theta}_s \cdot \mathbf{n} = \frac{B\phi_s^2}{Le_f} \bar{c} \exp\left(\frac{\bar{\theta}}{1 + \bar{\theta}/\gamma}\right) \quad \text{on } \partial\Omega_1 \quad (28)$$

$$\nabla \theta_s \cdot \mathbf{m} = 0 \quad \text{on } \partial\Omega_2 \quad (29)$$

The above model will be referred to as the Short Monolith (SM) model. More details about this model can be found in Balakotaiah et al. (2000). Again, it should be pointed out that this model is valid only for Peclet numbers less than unity ( $Pe < 1$ ). For a typical gas diffusivity of  $1 \text{ cm}^2/\text{s}$  and inlet gas velocity of  $10 \text{ m/s}$ , the SM model can be applied to a reactor whose length does not exceed  $10 \text{ }\mu\text{m}$ . For a gas velocity of  $1 \text{ m/s}$ , the SM model is valid for reactors of length smaller than  $100 \text{ }\mu\text{m}$ . Thus, the Short Monolith model is applicable for catalytic gauze reactors.

### The Convection Model

This model was first proposed by Damköhler (1937) and has been studied in previous literature (Heck et al., 1976; Young and Finlayson, 1976) for some geometries. It ignores the axial conduction (diffusion) terms (convection time and the transverse diffusion time are much smaller compared to the longitudinal diffusion time) and uses the Dirichlet boundary conditions at the inlet. In this case, the axial Peclet number is very high ( $Pe \rightarrow \infty$ ). The steady-state Convection model can be written as

$$f(x, y) \frac{\partial c}{\partial z} = \frac{1}{P} \nabla^2 c \quad \text{in } \Omega_1 \quad (30)$$

$$f(x, y) \frac{\partial \theta}{\partial z} = \frac{Le_f}{P} \nabla^2 \theta \quad \text{in } \Omega_1 \quad (31)$$

$$0 = \nabla^2 \theta_s \quad \text{in } \Omega_2 \quad (32)$$

with the boundary conditions at the inlet changed to

$$c = 1 \quad z = 0 \quad (33)$$

$$\theta = 0 \quad z = 0 \quad (34)$$

and the wall boundary conditions remaining the same (Eqs. 20 to 22). This model is valid for Peclet numbers  $Pe \gg 1$  and aspect ratio  $\alpha \rightarrow 0$  or equivalently,  $P/Pe \ll 1$ . For typical values of  $D_m = 1 \text{ cm}^2/\text{s}$ ,  $\langle u \rangle = 10 \text{ m/s}$ , and  $R_\Omega = 1 \text{ mm}$ , this model is valid if  $L > 10 \text{ cm}$  (or  $\alpha < 0.01$ ).

### Local and Circumferentially Averaged Mass (and Heat) Transfer Coefficients

As stated in the introduction, mathematical models of convection with diffusion in 3-D are simplified by using the concept of an effective transfer coefficient between the bulk fluid and the surface. This eliminates the transverse coordinates and leads to the simplified two-phase models. The effective transfer coefficients are often expressed in dimensionless form in terms of the Sherwood and Nusselt numbers. In this section, we concentrate on obtaining the mass (heat) transfer coefficient along the channel length and perimeter and also discuss the influence of the local Damköhler number ( $\phi_s^2$ ) on the transfer coefficients using the Convection and the Short Monolith models.

The mass (heat) transfer coefficient varies along the channel perimeter and also varies with axial position (for the case of the Convection model). The average Sherwood number (dimensionless mass transfer coefficient) at any cross section is defined by

$$Sh_{avg} = \frac{4k_{c,avg}R_\Omega}{D_m} = \frac{-4 \int_{\partial\Omega_1} \nabla c \cdot \mathbf{n} dS}{c_m - \int_{\partial\Omega_1} c_s dS} \quad (35)$$

where  $k_{c,avg}$  represents the average mass transfer coefficient and  $c_m$  is the dimensionless cup-mixing concentration in the fluid phase, defined by

$$c_m = \frac{\int_{\Omega_1} c(x, y) f(x, y) dA}{\int_{\Omega_1} f(x, y) dA} \quad (36)$$

and  $c_s$  is the dimensionless surface concentration. The local Sherwood number (which varies along the channel perimeter) is given by

$$Sh_{loc}(x, y) = \frac{4k_c(x, y)R_\Omega}{D_m} = \frac{-4 \nabla c(x, y) \cdot \mathbf{n}(x, y)|_{\partial\Omega_1}}{c_m - c_s(x, y)} \quad (37)$$

The average Nusselt number (dimensionless heat transfer coefficient) at any cross section is defined by

$$Nu_{avg} = \frac{4h_{avg}R_\Omega}{k} = \frac{-4 \int_{\partial\Omega_1} \nabla \theta \cdot \mathbf{n} dS}{\theta_m - \int_{\partial\Omega_1} \theta_s dS} \quad (38)$$

where  $h_{avg}$  represents the average heat transfer coefficient and  $\theta_m$  is the dimensionless cup-mixing temperature in the fluid phase defined by

$$\theta_m = \frac{\int_{\Omega_1} \theta(x, y) f(x, y) dA}{\int_{\Omega_1} f(x, y) dA} \quad (39)$$

and  $\theta_s$  is the dimensionless surface temperature.

The above definition of the Sherwood number is used to calculate the mass transfer coefficient using the isothermal version of the above models. The isothermal version of the above models can be obtained by dropping the energy balance and simplifying the boundary conditions. These partial differential equations are then solved for different geometries using the software package FEMLAB© (Comsol AB, Version 2.3.0.148, 2003) to obtain the Sherwood number. These calculations are repeated for different values of the local Damköhler number ( $\phi_s^2$ ) to obtain its influence on the Sherwood number. It should be pointed out that all the calculations in this work are done for the case of fully developed laminar velocity profile and thus the simplified Navier–Stokes equations (Eqs. 23a–23c) are solved first to obtain the function  $f(x, y)$ . For the case of the Short Monolith model, the isothermal model equations are given by

$$\frac{1}{P} \nabla^2 \bar{c} = f(x, y)(\bar{c} - 1) \quad \text{in } \Omega_1 \quad (40)$$

$$-\nabla \bar{c} \cdot \mathbf{n} = \phi_s^2 \bar{c} \quad \text{on } \partial\Omega_1 \quad (41)$$

where the parameters are evaluated at the reference temperature  $T_o$ . The above partial differential equation is solved for different geometries and Eqs. 35 and 37 are used to calculate the average and local Sherwood numbers. Figure 2 shows a plot of the local Sherwood number ( $Sh_{loc}$ ) along the perimeter of a geometry (square, triangular, rectangular, hexagonal, and sinusoidal ducts) for one set of parameters,  $\phi_s^2$  and  $P$ . The perimeter is normalized to unity and the Sherwood number is plotted starting from the bottom right corner and going around clockwise. As can be seen, the mass transfer coefficient is not a constant along the channel perimeter and is low at the corners and is maximum midway along the side. The mass transfer coefficient is small as we approach the corners because the difference between the cup-mixing concentration and the surface concentration is high (attributed to higher diffusion length) and the flux is very low at the corners. (Note: The outward normal is not defined for sharp corners. In such cases, the boundary condition Eq. 41 was used to approximate the flux.) Rectangular channels have a higher transfer coefficient along the side with higher dimensions compared to the side with lower dimensions. For sinusoidal channels, the Sherwood number is small near the corners (the sharp and rounded corners) and has maxima (two of them) along the sinusoidal surface. Table 1 shows the various geometries (with dimensions) with



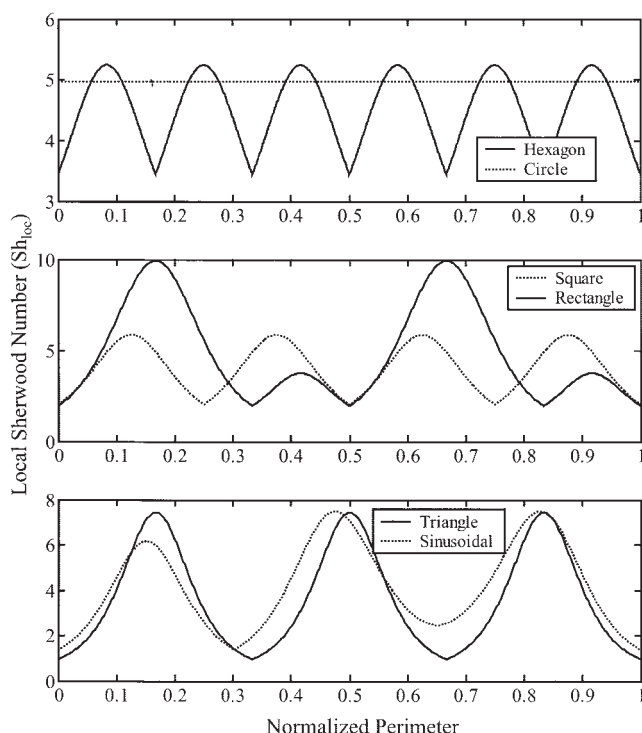


**Figure 2. Variation of the local Sherwood number along the perimeter for different channel geometries for the Short Monolith model. Parameters values:  $\phi_s^2 = 1$ ,  $P = 1$ .**

the corresponding average asymptotic Nusselt and Sherwood numbers.

The dependency of the average Sherwood number on the transverse Peclet number ( $P$ ) is interesting. We vary the transverse Peclet number and plot the average Sherwood number as a function of  $P^{-1}$ . (This is the Graetz coordinate often used in the heat and mass transfer literature.) A typical plot for triangular geometry for different values of the transverse Thiele modulus ( $\phi_s^2$ ) is shown in Figure 3. There are two asymptotes for large and small values of  $P$ . For very small values of  $P$ , the Sherwood number reaches a constant asymptotic value and is independent of  $P$  and for large values of  $P$ , the Sherwood numbers reach the other asymptote where it keeps increasing as the value of  $P$  increases. For very small values of  $Da (= \phi_s^2/P)$ , the Sherwood number does not depend on the local Damköhler number. Analytical expressions for the two asymptotes have been published for the case of circular geometry (for both laminar and flat velocity profiles) in the work by Gupta and Balakotaiah (2001). It is interesting to note that the numerical value of the constant asymptote is not a constant for all operating parameters as in the case of heat exchangers (and other heat transfer problems where the flux at the wall is a constant or the temperature at the wall is a constant) but depends on the local Damköhler number ( $\phi_s^2$ ).

We solve the partial differential equation for different values of the local Damköhler number ( $\phi_s^2$ ) for very small values of the transverse Peclet number ( $P$ ), to obtain the asymptotic average Sherwood number as a function of  $\phi_s^2$ . For very low values of  $\phi_s^2$ , the monolith reactor behaves as if the flux at the wall is a constant along the transverse and axial direction

[because we are neglecting axial gradients and considering very small values of the transverse Peclet number ( $P$ )]. From the heat transfer literature (Shah and London, 1978), we know that there are two different kinds of heat transfer boundary conditions for the case of constant heat flux along the axial direction. One is denoted by  $H_1$ , where the temperature is constant along the circumference, and the other is denoted by  $H_2$ , where the flux is constant along the circumference. For very low local Damköhler number ( $\phi_s^2$ ), the reaction time is large compared to the transverse diffusion time. Therefore, the flux along the circumference is almost constant (and small). It should be noted that because of the change in transverse diffusion length (distance from the center of the channel to the wall) along the channel perimeter and very slow reaction, the concentration along the channel perimeter is not a constant. For this case the average Sherwood number reaches the value corresponding to the  $H_2$  boundary condition. For very high  $\phi_s^2$ , the reaction is very fast (almost instantaneous) and thus the concentration along the channel perimeter is zero. Thus the average Sherwood number for high  $\phi_s^2$  for the Short Monolith model reaches the value corresponding to the  $H_1$  case. Thus, as the local Damköhler number increases from a very low value to a high value, the asymptotic Sherwood number shifts from the value corresponding to the  $H_2$  boundary condition to the value corresponding to  $H_1$  boundary condition.

Figure 4 shows this dependence of the average Sherwood number on the local Damköhler number for triangular, square, rectangular, sinusoidal, and hexagonal channel cross sections (for small values of  $P$ ). It should be noted here that for geometries (symmetrical ducts having constant peripheral curvature like circular ducts) where  $H_1$  and  $H_2$  are the same, the average Sherwood number for the Short Monolith model does not depend on the local Damköhler number. For square and hexagonal ducts, the  $H_1$  and  $H_2$  values are close and thus the variation with the local Damköhler number is smaller. Although the calculations done here are for the asymptotic average Sherwood number, similar trends are also found in the other asymptote (in which the Sherwood number depends on the value of  $P$ ). In the Short Monolith model, for small values of local Damköhler number the average Sherwood number is close to the value corresponding to the  $H_2$  boundary condition for all values of  $P$ , whereas for large local Damköhler number the average Sherwood number approaches the value corresponding to the  $H_1$  boundary condition.

Similar calculations can be done for the Convection model ( $Pe \rightarrow \infty$ ) to find the dependency of the average Sherwood number on the local Damköhler number and the variation of the Sherwood number along the channel length (Tronconi and Forzatti, 1992). The isothermal version of the Convection model may be written as



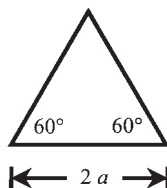
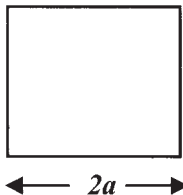
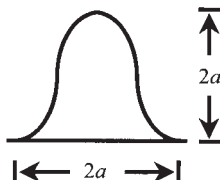
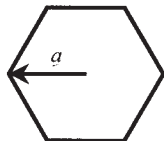
$$f(x, y) \frac{\partial c}{\partial z} = \frac{1}{P} \nabla^2 c \quad \text{in } \Omega_1 \quad (42)$$

$$c = 1 \quad z = 0 \quad (43)$$

$$-\nabla c \cdot \mathbf{n} = \phi_s^2 c \quad \text{on } \partial\Omega_1 \quad (44)$$

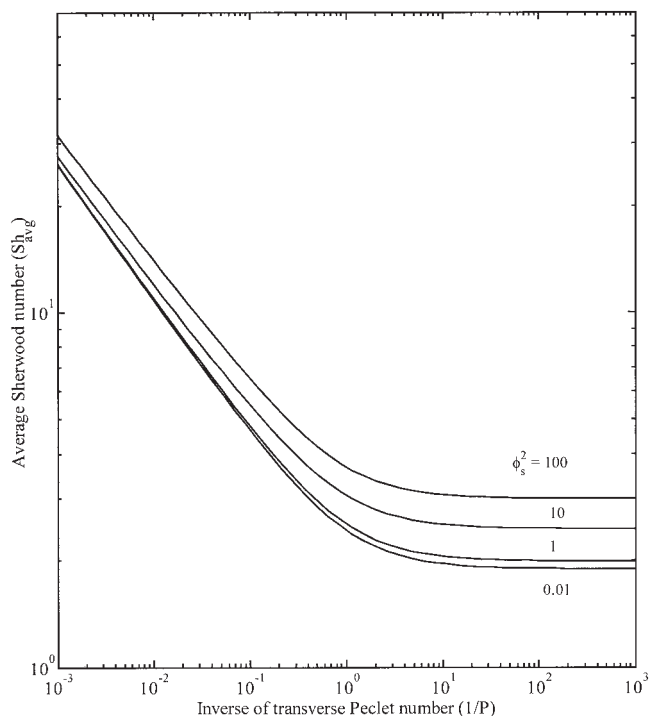
As can be expected, the local Sherwood number follows the same trend like in the Short Monolith model. The local Sher-

Table 1. Effective Diffusion Length and Asymptotic Constants for Some Common Channel Geometries

Channel Shape	$R_h(2R_\Omega)$	$Nu(Sh)_{H_{2,\infty}}$	$Nu(Sh)_{H_{1,\infty}}$	$Nu(Sh)_{T,\infty}$	$\alpha_1$
	$a$	4.364	4.364	3.656	0.81905
	$2a$	8.235	8.235	7.541	0.91035
	$\frac{a}{\sqrt{3}}$	1.893	3.111	2.497	0.7753
	$a$	3.089	3.608	2.977	0.8074
	$\frac{4a}{3}$	3.023	4.123	3.392	0.7891
	$\frac{3a}{2}$	2.97	4.795	3.956	0.7695
	$0.770a$	2.731	3.649	2.966	0.7872
	$\frac{\sqrt{3}}{2} a$	3.861	4.002	3.34	0.8156

wood number is very low at sharp corners and lower at places where the effective diffusion length is large. However, because the axial coordinate is not eliminated in the Convection model, the Sherwood number depends on the axial position. (Note:  $z/P$  is the Graetz coordinate used in the literature.) We solve the above partial differential equation as an initial value problem in FEMLAB after spatial discretization of the domain  $\Omega_1$ . The solution obtained is used to calculate the average Sherwood number along the axial coordinate. Figure 5 shows the variation of the average Sherwood number along the channel length for six different channel cross sections for one set of parameters. [The case of circular, square and triangular channels was already solved by Tronconi and Forzatti (1992) but is included here for completeness.] As expected, the mass transfer coefficient is very high near the inlet of the reactor (where the

concentration boundary layer is developing) and it approaches the asymptotic value further down the channel. We observe the same behavior for all the geometries. Again, as in the case of Short Monolith model, it is interesting to note that this asymptotic value depends on the local Damköhler number. However, as the local Damköhler number increases from a low to a high value, the asymptotic Sherwood number shifts from the  $H_2$  value to the  $T$  value (unlike the shift from  $H_2$  to  $H_1$  in the Short Monolith model). The  $T$  boundary condition corresponds to a case where the temperature/concentration at the wall is constant throughout the reactor (axially and circumferentially). For very low local Damköhler number ( $\phi_s^2$ ), the reaction is slow and the wall flux along the channel perimeter and in axial direction is constant (throughout the channel) and thus the Sherwood number reaches the value corresponding to the  $H_2$



**Figure 3.** Variation of the average Sherwood number for the Short Monolith model with the transverse Peclet number for different values of the Damköhler number for triangular channels.

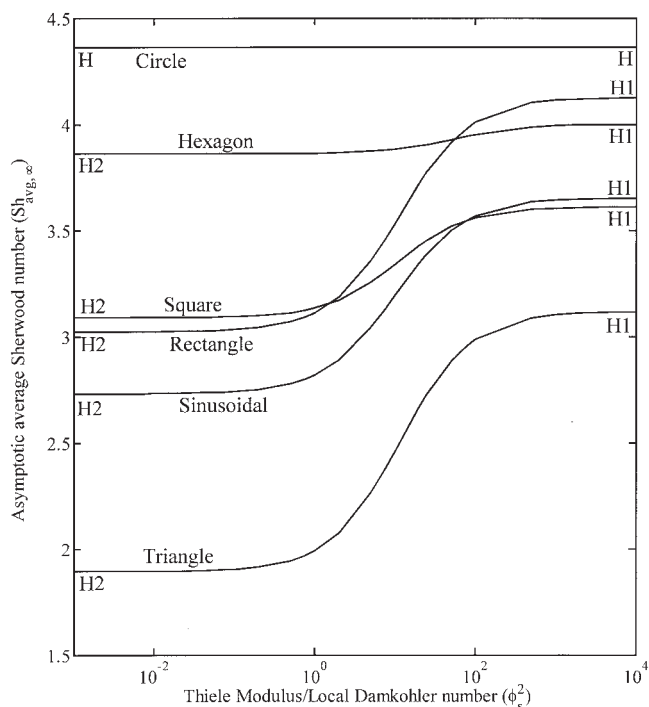


**Figure 4.** Variation of the average asymptotic Sherwood number with the local Damköhler number for the Short Monolith model for  $P = 0.01$ .

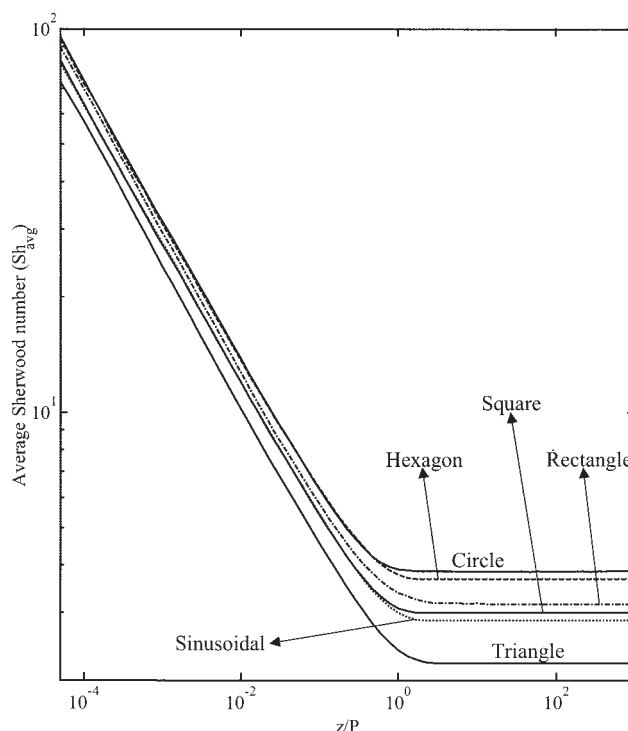


**Figure 5.** Dependency of the average Sherwood number on  $z/P$  for the Convection model for different geometries for  $\phi_s^2 = 10$ .

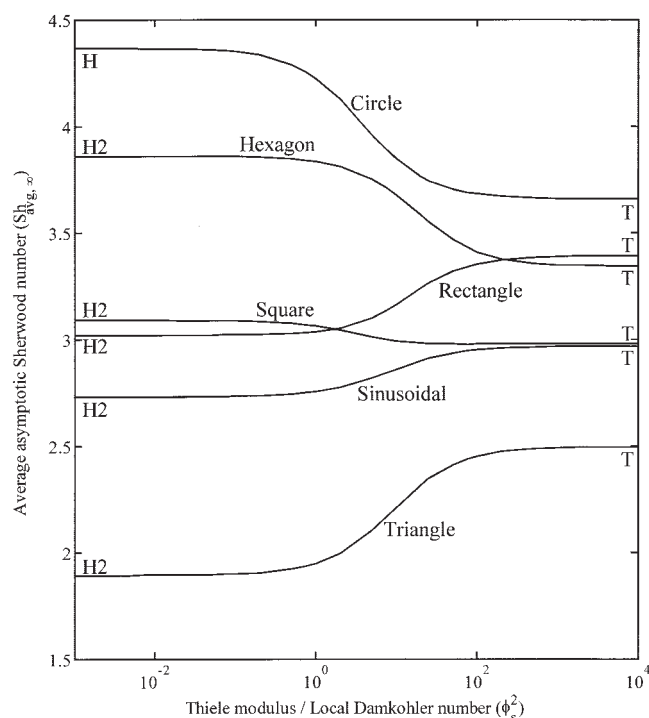
boundary condition. For high  $\phi_s^2$ , the reaction is very fast and the wall concentration is close to zero along the channel perimeter. Because the reaction is fast and the asymptotic Sherwood number is reached further down the monolith, the concentration would be small along the axial direction also (as the reactant would be used up for the fast reaction). Thus for this case the asymptotic average Sherwood number reaches the value corresponding to the  $T$  case.

Figure 6 shows this effect of the local Damköhler number on the average asymptotic Sherwood numbers for different ducts. Although we are analyzing only the average asymptotic Sherwood number corresponding to the constant (small  $P$ ) asymptote, it is easily seen that the same trends will be followed in the other asymptote also. Therefore, for low values of the local Damköhler number, the transfer coefficients will be closer to the values corresponding to the  $H_2$  boundary condition throughout the reactor (although it will be somewhat higher near the inlet).

The above calculations have been made using the isothermal models. It should be pointed out that the solid phase conduction does not affect the results of the isothermal model. Similar calculations are done for the case of nonisothermal models with peripheral conduction in the solid included. The influence of the peripheral solid conduction on the transfer coefficients is also studied. The Short Monolith model, governed by Eqs. 24–26 and boundary conditions 27–29, is solved for various values of the local Damköhler number ( $\phi_s^2$ ).

Figure 7 shows a plot of the average asymptotic Nusselt number as a function of the local Damköhler number for various values of  $\kappa$  ( $=k_s/k_p$ ) and  $\delta = 0.44$ . It should be pointed out here that the wall thickness does not influence the steady-





**Figure 6. Variation of the average asymptotic Sherwood number with the local Damköhler number for the Convection model for  $P = 1$ .**

state solutions of the models presented here. As can be seen, for very low solid conduction the influence of the local Damköhler number ( $\phi_s^2$ ) on the Nusselt number is very similar to the influence of the local Damköhler number on the Sherwood number discussed above. For very low values of the local Damköhler number ( $\phi_s^2$ ), the Nusselt number reaches the  $H_2$  asymptote and for high values of the local Damköhler number, the Nusselt number reaches the  $H_1$  asymptote. However, as the solid conduction is increased, the asymptotic value for low values of the local Damköhler number ( $\phi_s^2$ ) shifts from  $H_2$  to  $H_1$  value. (Note: It should be mentioned that there are small jumps in the transfer coefficients at ignition points that are smoothed out in Figure 7. These jumps occur because of the Gibbs phenomenon, which is explained in detail later.) As solid conduction increases, the wall temperature becomes more uniform and thus the Nusselt number approaches the value corresponding to the  $H_1$  boundary condition. It is interesting to note that on the quenched branches (or kinetic regime) the ratio  $\kappa$  need to be of the order of  $10^6$  for the Nusselt number to reach the  $H_1$  boundary condition, even though for all practical purposes  $\kappa > 10$  gives close to uniform temperature along the channel perimeter (see next section). On the ignited branch ( $\phi_s^2 > 10$ )  $Nu_{avg}$  is nearly independent of  $\kappa$  and is close to  $Nu_{H_1}$ .

Similar trends are also seen in the Convection model. For very low values of the local Damköhler number ( $\phi_s^2$ ), the Nusselt number changes from  $H_2$  to  $H_1$  value as the solid conduction is increased. For very high values of the local Damköhler number ( $\phi_s^2$ ), however, the Nusselt number reaches the  $T$  asymptote. Thus depending on the value of  $\kappa$ , the Nusselt number starts with a value between  $H_2$  and  $H_1$  boundary condition type for low local Damköhler number ( $\phi_s^2$ ) and

reaches the  $H_1$  ( $T$ ) asymptote for high values of the local Damköhler number for the Short Monolith (Convection) model. It should be pointed out here that the Sherwood number behavior remains unaffected and always starts with the  $H_2$  value for low local Damköhler number ( $\phi_s^2$ ) and reaches the  $H_1$  ( $T$ ) asymptote for high values of the local Damköhler number for the Convection model. It should be pointed out that for channels with constant peripheral curvature, the solid conduction does not have any influence on the Nusselt number.

For any finite value of the axial Peclet number ( $Pe$ ), similar trends can be expected for the dependency of the asymptotic average Sherwood and Nusselt number on the local Damköhler number. For very low local Damköhler numbers the asymptotic Sherwood number will reach the  $H_2$  value and for very large local Damköhler numbers, the asymptotic value will be between  $H_1$  (for  $Pe \rightarrow 0$ ) and  $T$  (for  $Pe \rightarrow \infty$ ) value depending on the axial Peclet number. For very low local Damköhler numbers the asymptotic Nusselt number will reach a value between  $H_2$  and  $H_1$  depending on the value  $\kappa$  and for very large local Damköhler numbers, the asymptotic value will be between  $H_1$  (for  $Pe \rightarrow 0$ ) and  $T$  (for  $Pe \rightarrow \infty$ ) value depending on the axial Peclet number. The bounds on the Nusselt numbers are shown in Figure 8 for triangular ducts for some limiting cases. For any finite axial  $Pe$  and finite  $\kappa$ , the Nusselt number variation with the local Damköhler number is bounded between the curves shown for  $Pe \rightarrow \infty$ ,  $\kappa = 0$ , and  $Pe \rightarrow 0$ ,  $\kappa \rightarrow \infty$ .

In the Convection model, as we move further down the

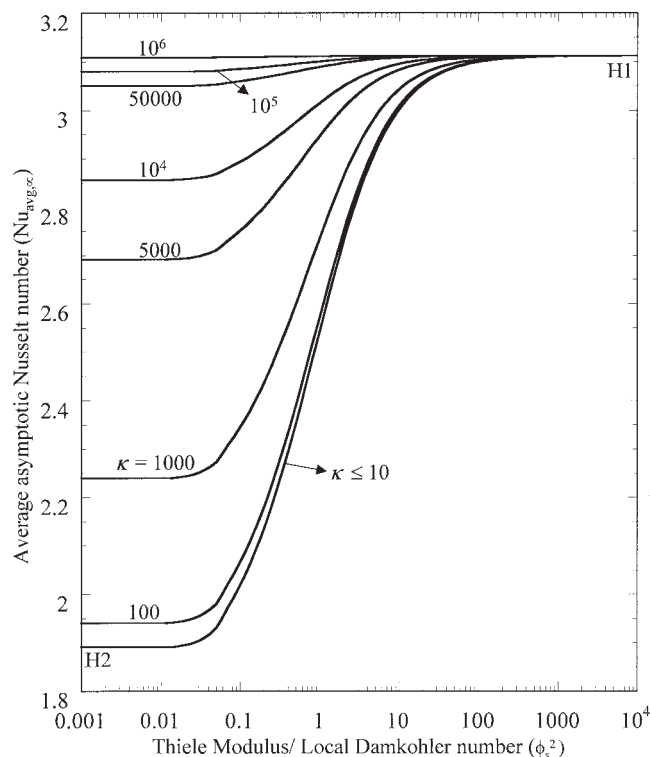


**Figure 7. Variation of the average asymptotic Nusselt number with the local Damköhler number for the Short Monolith model with triangular channels for  $P = 0.001$ ,  $B = 10$ ,  $\gamma = 25$ ,  $Le_r = 1$ , and for different ratios of solid to fluid thermal conductivities.**

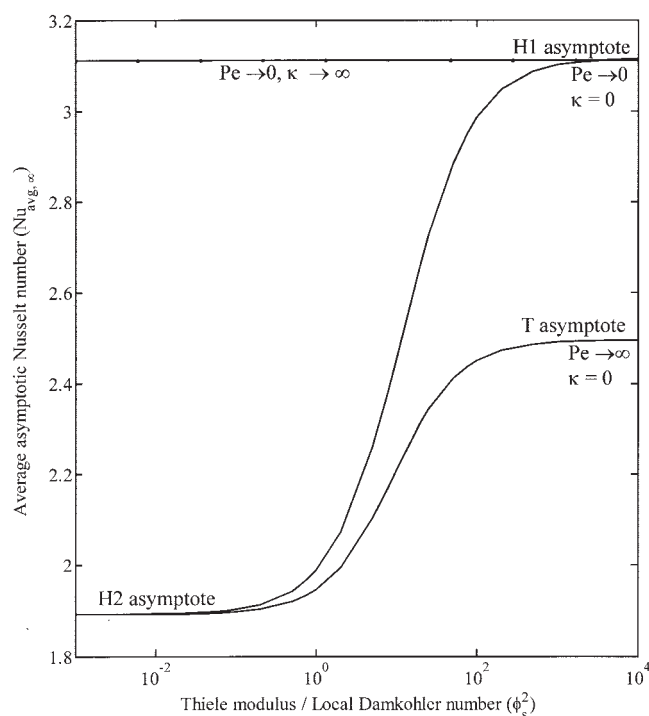


**Figure 8. Variation of the average asymptotic Nusselt number with the axial Peclet number and the local Damköhler number for triangular channels.**

channel, the effective local Damköhler number ( $\phi_s^2$ ) keeps changing (increasing) as the reaction progresses. The asymptotic Sherwood/Nusselt number is bounded between the values corresponding to the slow (low  $\phi_s^2$ ) and fast reaction (high  $\phi_s^2$ ) cases. The Sherwood/Nusselt number starts with the value corresponding to the  $H_2$  boundary condition and reaches the value corresponding to the  $T$  boundary condition as the reaction progresses (or along the axial coordinate). The nonisothermal Convection model, represented by Eqs. 30 to 34 with the boundary conditions represented by Eqs. 20 to 22, is solved using an initial value approach using FEMLAB for the case of zero solid conduction as in the case of the isothermal model. Figures 9 and 10 show the variation of the Nusselt number in a monolith calculated using the Convection model for circular and triangular channels, respectively.

Also shown in the figures are the bounding curves for the Nusselt numbers corresponding to the  $H_1$ ,  $H_2$ , and  $T$  boundary conditions. The figure shows a sharp peak in the Nusselt number plot (and a similar one is also seen in the Sherwood number plot). It also shows that the computed curve has some numerical error as it lies outside the bounds for small  $z$ . Similar results have also been shown in previous studies (Heck et al., 1976; Young and Finlayson, 1976). It has been shown by Gupta and Balakotaiah (2001), however, that the local maximum in the heat/mass transfer coefficient is a result of numerical inaccuracies associated with the Gibbs phenomenon that occurs in the series expansion of a discontinuous function. The actual wall temperature  $\theta_w$  variation along the channel length has a jump discontinuity (attributed to ignition on the surface), which is approximated by a continuous profile in the initial

value approach. This is because the nonisothermal case is fundamentally different from the isothermal case in the sense that the local heat balance, given by Eq. 21, can have multiple solutions at some axial distance depending on the surface temperature. These multiple solutions cannot be obtained using the IVP approach. [Further details about the Gibbs phenomenon and the discontinuity in the transfer coefficients can be found in Gupta and Balakotaiah (2001).] Once the reaction is ignited, the surface temperature jumps and thus the local Damköhler number is very high after ignition. This high value of the local Damköhler number shifts the Sherwood/Nusselt number corresponding to the  $T$  boundary condition. For low values of the local Damköhler number, the Nusselt number corresponds to the  $H_2$  asymptote and shifts to the  $T$  asymptote as the reaction ignites. Thus, the Nusselt number should be bounded between the  $H_2$  and the  $T$  asymptotes.

As can be seen in Figure 9 for a circular channel, the Nusselt number starts with the  $H_2$  asymptote but because of the Gibbs phenomenon  $Nu_{avg}$  overshoots and then reaches the  $T$  asymptote. Triangular channels do not have a uniform ignition around the channel perimeter and it is seen that ignition first occurs at the corners (explained in detail in the next section). As shown in Figure 10, for triangular channels,  $Nu_{avg}$  starts with the  $H_2$  asymptote and once ignition occurs at the corner, there is an upward jump and then it attains the  $T$  asymptote once the entire perimeter is ignited. It is important to note that in the case of circular channels the Nusselt number is supposed to have a downward jump from  $H$  to  $T$  (as  $Nu_H > Nu_T$ ) but the calculated Nusselt number overshoots and then reaches the  $T$  asymptote.

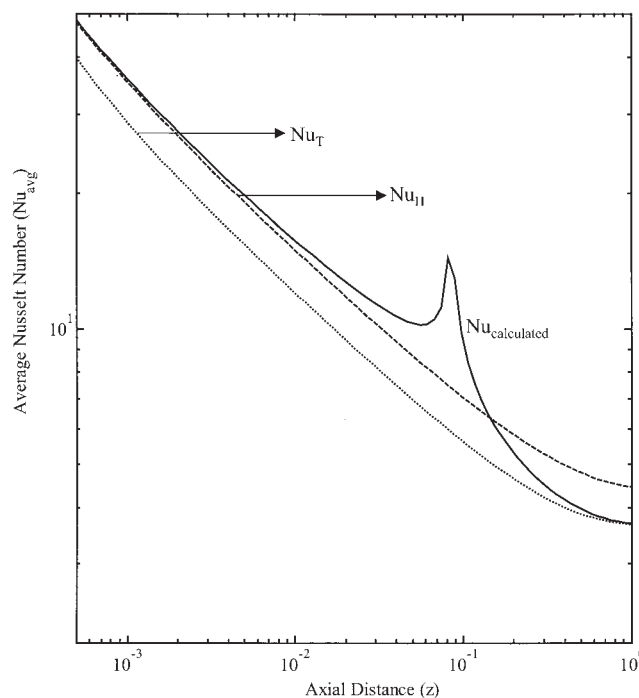


**Figure 9. Variation of the average Nusselt number with the axial coordinate for the Convection model for circular channels for parameter values  $B = 10$ ,  $Le_f = 1$ ,  $\gamma = 25$ ,  $P = 1$ ,  $\phi_s^2 = 0.1$ ,  $\theta_{in} = 0$ ,  $\kappa = 0$ .**

The maximum in  $Nu$  is spurious and is attributed to numerical inaccuracy associated with the Gibbs phenomenon.

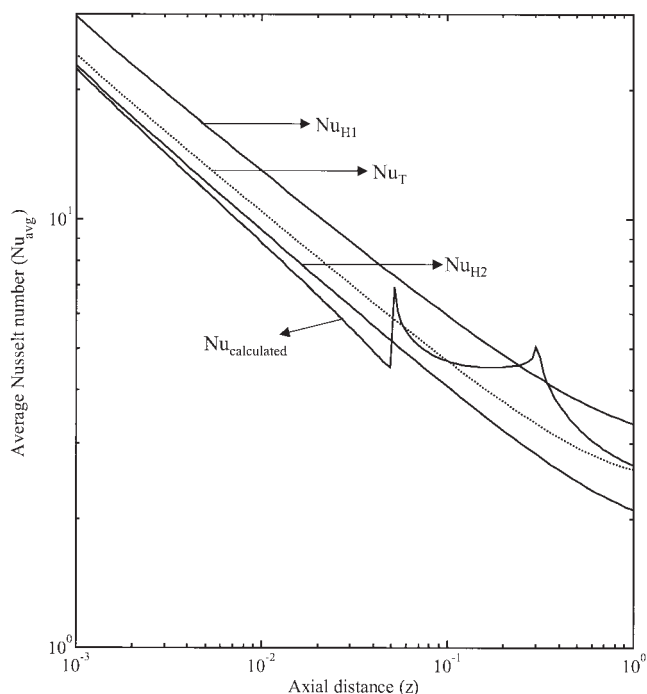


**Figure 10.** Variation of the average Nusselt number with the axial coordinate for the Convection model for triangular channels for parameter values  $B = 10$ ,  $Le_f = 1$ ,  $\gamma = 25$ ,  $P = 1$ ,  $\phi_s^2 = 0.03$ ,  $\theta_m = 0$ ,  $\kappa = 0$ .

The local maxima and minima in Nu are inaccurate because of the Gibbs phenomenon.

In the case of triangular channels  $Nu_{H_2} < Nu_T$ , however, and thus the Nusselt number is supposed to have an upward jump. As can be seen from the plot, there is an upward jump and the Gibbs phenomenon is not as pronounced here.

Figure 11 shows plots of the numerically calculated heat flux at the wall and the temperature difference between the wall and fluid. As can be seen, for circular channels, at ignition, the wall temperature undergoes a sudden jump to the ignited value. (The true solution has a discontinuous jump but it is approximated by a continuous function in the numerical solution.) A similar behavior can be seen for the heat flux. However, for triangular channels, given that ignition is nonuniform along the channel perimeter, the jump in the average solid temperature is not very high and the Gibbs phenomenon is not as pronounced (but is still present, as can be seen in Figure 10). The average solid temperature does not spike much in triangular channels (compared to circular channels) in a small distance, even though the corners are ignited. Thus the actual variation of the Nusselt/Sherwood number in a triangular monolith starts with the  $H_2$  asymptote and jumps to the  $T$  asymptote once the monolith is ignited. For circular channels, this jump from  $H_2$  to  $T$  occurs at a point, whereas for triangular channels, the transition from  $H_2$  to  $T$  asymptote is spread over a small distance (because of the nonuniform ignition along the channel perimeter). If axial conduction/diffusion is included in the model, the Nusselt/Sherwood number would have values close to the  $H_2$  boundary condition near the inlet of the reactor and as we move in the axial direction these values decrease in the axial direc-

tion. At the ignition point, the Nusselt/Sherwood numbers shift from the  $H_2$  asymptote to a value between the  $H_1$  ( $Pe \rightarrow 0$ ) and  $T$  ( $Pe \rightarrow \infty$ ) asymptotes depending on the value of axial Peclet number.

The Nusselt/Sherwood numbers in the 1-D two-phase models that are used in the modeling of monoliths and other catalytic reactors are the asymptotic values. The above analysis shows that the transfer coefficients can vary along the axial direction, reach different asymptotes depending on the axial Peclet number, and jump from one value to another at ignition. A simple expression for the transfer coefficients thus cannot be obtained for all values of  $\phi_s^2$ ,  $P$ ,  $\gamma$ ,  $B$ ,  $Le_f$ , and  $Pe$ . Also, it is usually not known beforehand where the ignition occurs [although it can be predicted to some extent using the analytical ignition criterion given in Ramanathan et al. (2003)] and thus the jump in the transfer coefficients cannot be incorporated. Based on the calculations and analysis presented here, we observe that for an exothermic wall reaction in a catalytic monolith the transfer coefficients always start with the value corresponding to the  $H_2$  boundary condition and jump to a value between the  $T$  boundary condition and  $H_1$  boundary condition as we move in the axial direction. (Note: The asymptotic Nusselt/Sherwood number in an ignited part of the reactor is always going to be a number that lies between the values corresponding to the  $H_1$  and  $T$  boundary conditions.)

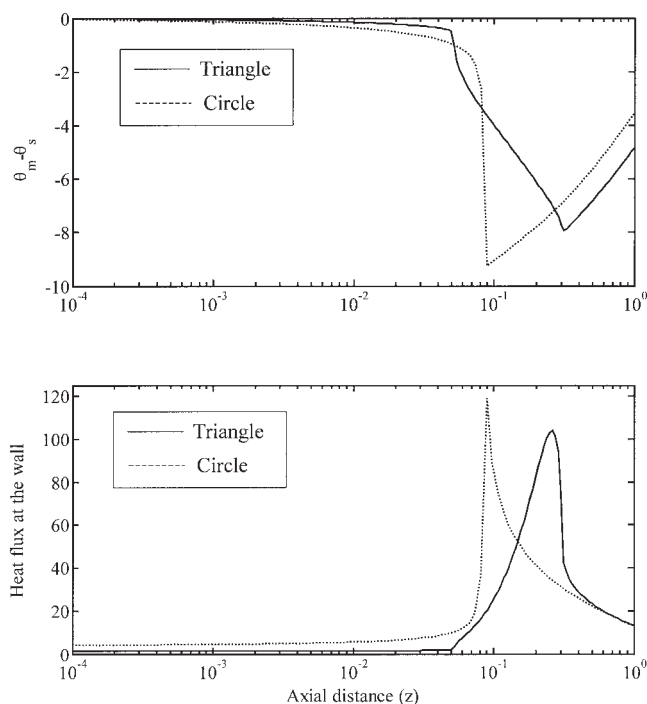


**Figure 11.** Variation of the temperature difference and the heat flux with the axial coordinate for the Convection model for circular channels and triangular channels for parameter values  $B = 10$ ,  $Le_f = 1$ ,  $\gamma = 25$ ,  $P = 1$ ,  $\kappa = 0$ ,  $\theta_m = 0$ ,  $\phi_s^2 = 0.1$  (Circle),  $0.03$  (Triangle).

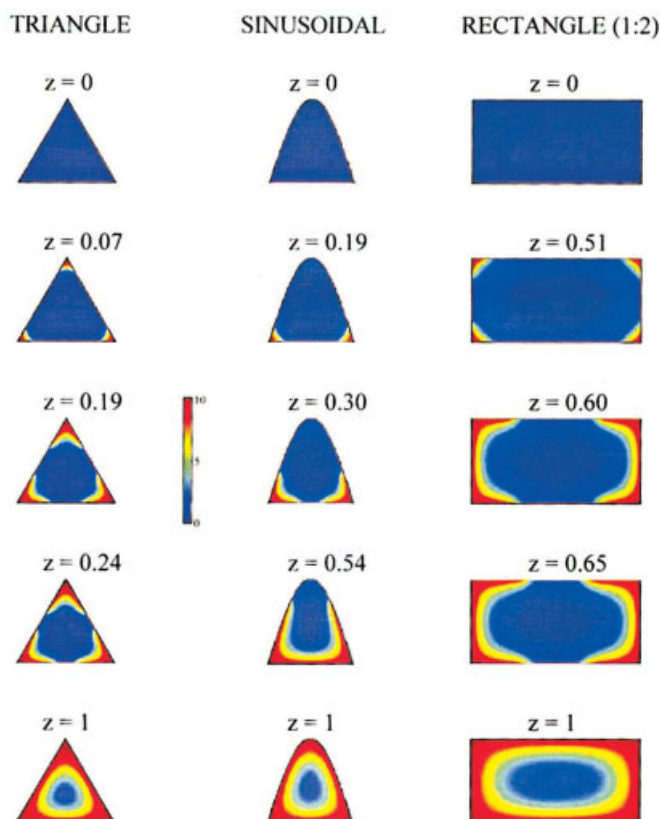


**Figure 12.** Temperature plots obtained using the Convection model, which shows the ignition behavior in triangular, sinusoidal, and rectangular channels for parameter values  $B = 10$ ,  $\phi_s^2 = 0.03$ ,  $\gamma = 25$ ,  $Le_f = 1$ ,  $P = 1$ ,  $\theta_{in} = 0$ ,  $\kappa = 0$ .

### Ignition Behavior and Conversion in the Mass Transfer Controlled Regime

For symmetrical ducts with constant peripheral curvature (circular and parallel-plate channels), the transverse diffusion length is the same for all points on the wall so the channel wall is heated uniformly and ignition occurs uniformly around the channel. However, for all other channel shapes the heat transfer rate varies in the circumferential direction (because the transverse diffusion length is not constant on the circumference) and ignition occurs first near the corners (where the heat transfer coefficient is lowest and transverse diffusion length is largest). This behavior is verified using the Convection model. Figure 12 shows plots of the temperature profiles in triangular, sinusoidal, and rectangular geometries along the channel length for the Convection model with zero solid conduction. Though not shown here explicitly, we find similar behavior for other geometries (square and hexagonal ducts). For all the geometries with corners, ignition occurs first at the corners and then spreads along the channel perimeter. It should be pointed out that during ignition, the difference between the maximum and minimum temperature along the channel perimeter can be as high as the dimensionless adiabatic temperature increase ( $B$ ). The maximum temperature is usually at the corners, where the transfer coefficients are small and the minimum temperature will be somewhere in the middle along one of the sides where the transfer coefficients are high.

In an earlier work, Ramanathan et al. (2003) derived an analytical ignition criterion using a one-dimensional two-phase model to predict the nature of ignition in catalytic monoliths. For the case of wall reaction (or no washcoat diffusional limitations), the ignition criterion may be expressed as

$$\frac{B\phi_s^2}{P} + \frac{4eB\phi_s^2}{Le_f Nu_{H,\infty}} > 1 \quad (45)$$

The first term in the above criterion represents the ignition locus of the homogeneous or pseudohomogeneous plug flow model and the heterogeneous contribution (or local ignition) appears through the second term. If the first term exceeds unity and the second term is negligible (compared to unity) we have a back-end ignition, which is always the case for a pseudohomogeneous model. If the second term exceeds unity, we have a front-end ignition irrespective of the contribution from the first term. For the case where the sum exceeds unity, with the second term less than unity and not negligible compared to the first term, then we have a middle ignition. The one-dimensional model is obtained by averaging across a given cross section (in the transverse direction) and thus the detailed information about the channel geometry is lost. The effect of channel geometry in a one-dimensional two-phase model comes only through the circumferentially averaged heat and mass transfer coefficients. As pointed out earlier, the heat and mass transfer coefficients have a lower value at the corners and using this lower value in the ignition criterion would mean that the monolith would ignite more easily than using the average value. For parameter values where the second term is much smaller than unity, the effect of channel geometry on ignition is negligible and all channel cross sections behave the same way (and will have the same ignited length), although different channel shapes give different conversions depending on the asymptotic Sherwood numbers. Thus by choosing the parameter values appropriately, we could either minimize the geometry effect (for example, choosing parameter values such that the second term is very small) or we could have a strong influence of channel geometry on ignition (for example, when the second term is closer to unity).

The value of the average asymptotic Nusselt number in the second term of the ignition criterion can either be the value corresponding to the  $H_1$  boundary condition or  $H_2$  boundary condition. If the criterion is satisfied using the  $H_1$  boundary condition value, all the points along the channel perimeter are ignited. If the criterion is satisfied using the  $H_2$  boundary condition value (and is not satisfied using the  $H_1$  boundary condition), then there is local ignition only near the corners and the entire perimeter is not ignited. In a 1-D model, we average out the peripheral variations and by *ignition* we mean that the entire channel perimeter is ignited. Thus using the  $H_1$  boundary condition value is the most appropriate when we consider the 1-D model. If we are interested in local ignition (near the corners) then we could use the  $Nu_{H_2}$  value in Eq. 45 to find the minimum catalyst loading required for ignition. When the ignition criterion is written as

$$\frac{B\phi_s^2}{P} + \frac{4eB\phi_s^2}{Le_f Nu_{H_1,\infty}} > 1 \quad (46)$$



it implies that all points along the circumference of the channel are ignited. Also, to predict ignition/extinction behavior using simplified two-phase models, it is a good practice to use the values corresponding to the  $H_1$  boundary condition for the transfer coefficients. This will always give the qualitative features correctly but may give some error in the numerical values of temperature and concentration on the ignited branch. If the inlet temperature is so high that the entire channel is in the mass transfer controlled regime, then the transfer coefficients corresponding to the  $T$  boundary condition are more appropriate. [Note: As mentioned in the previous section, we observe that for an exothermic wall reaction in a catalytic monolith the transfer coefficients always start with the value corresponding to the  $H_2$  boundary condition and jump to a value (at ignition) between the  $T$  boundary condition and  $H_1$  boundary condition as we move in the axial direction. However, when the 3-D model is simplified, we assume that the variations of temperature and concentration in the transverse direction are small and thus it would be reasonable to use the  $H_1$  values instead of  $H_2$  values to predict the ignition behavior in the monolith.]

Also, with the help of the ignition criterion, we can choose the parameters so that some channel cross sections have ignition and others do not. Figure 13 shows a plot of the averaged wall temperature  $\theta_{w,avg}$  (averaged along the channel perimeter at a given cross section) for a set of parameters (with zero solid conduction) where ignition occurs in triangular, sinusoidal, square, and rectangular channels and there is no ignition in circular or hexagonal channels. The average solid or wall temperature is given by

$$\theta_{w,avg}(z) = \frac{\int_{\partial\Omega_1} \theta(x, y) dS}{P_{\Omega_1}}$$

Figure 14 shows a plot of the maximum wall temperature (which is at the corners) for the same set of parameters. In triangular channels the corners ignite at an axial distance of  $z = 0.05$  and the ignition front starts spreading in the axial and azimuthal directions. At a distance of  $z = 0.3$  (from Figure 13) the entire perimeter is ignited. Similar observations can be made for sinusoidal, rectangular, and square geometries. This clearly shows that the average and the maximum wall temperature (at the corners) differ considerably in channels with sharp corners when  $\kappa = 0$ .

In Figure 15 we compare the average solid or wall temperature along the monolith channel for different channel geometries. As can be seen, the triangular and sinusoidal channels ignite much earlier compared to circular channels. Square and rectangular channels ignite almost at the same length. (Note: The comparison made here is for channels with the same average effective transverse diffusion length.) From Figure 15 it is clear that triangular channels have a larger ignited length (around 88% of the channel length) and circular channels have only around 45% of the channel length ignited. For the set of parameters used, triangular, sinusoidal, square, rectangular, hexagonal, and circular channels have 55.5, 58.5, 57.6, 60.6, 53.6, and 49.9% conversion, respectively.

In some applications (such as automobile exhaust catalytic converters), we not only want to have ignition sooner (or a larger ignited length), but also need to have a good exit conversion in the mass transfer controlled regime. If the average

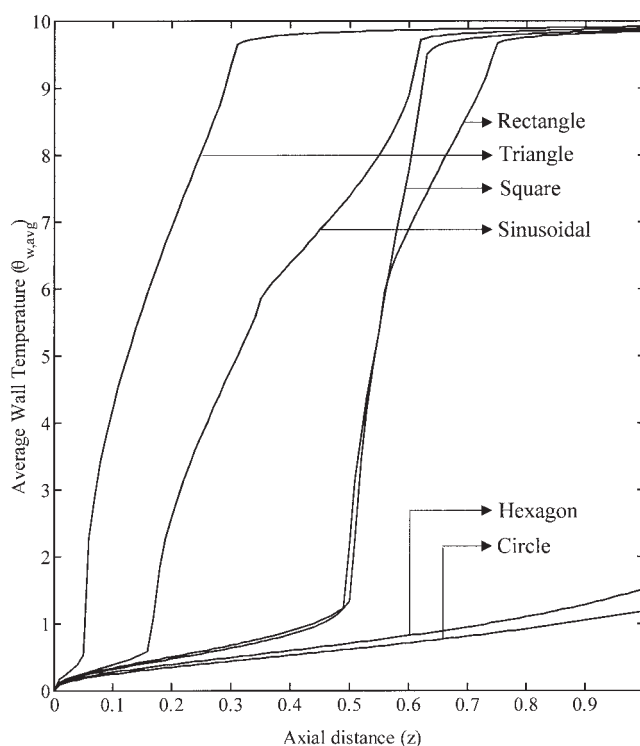


**Figure 13.** Average surface/wall temperature along the axial distance obtained using the convection model for different channel geometries for parameter values  $B = 10$ ,  $\phi_s^2 = 0.03$ ,  $\gamma = 25$ ,  $Le_f = 1$ ,  $P = 1$ ,  $\theta_{in} = 0$ ,  $\kappa = 0$ .

wall concentration is much less than the cup-mixing concentration then the monolith is locally in the mass transfer controlled regime. The average solid or wall concentration is given by

$$c_{s,avg} = \frac{\int_{\partial\Omega} c(x, y) dS}{P_{\Omega}}$$

and is related to the cup-mixing concentration by

$$c_{s,avg} = \frac{c_m}{1 + \frac{\phi_s^2}{Sh_{avg}(z)} \exp\left(\frac{\theta_{w,avg}}{1 + \frac{\theta_{w,avg}}{\gamma}}\right)} \quad (47)$$

where  $Sh_{avg}(z)$  is the average Sherwood number at an axial distance  $z$  from the channel inlet. For the monolith to be in the mass transfer controlled regime we will need the second term in the denominator of Eq. 47 to be much greater than unity. As a practical criterion, we can take

$$\frac{\phi_s^2}{Sh_{avg}(z)} \exp\left(\frac{\theta_{w,avg}}{1 + \frac{\theta_{w,avg}}{\gamma}}\right) \geq 10 \quad (48)$$

for mass transfer controlled operation.



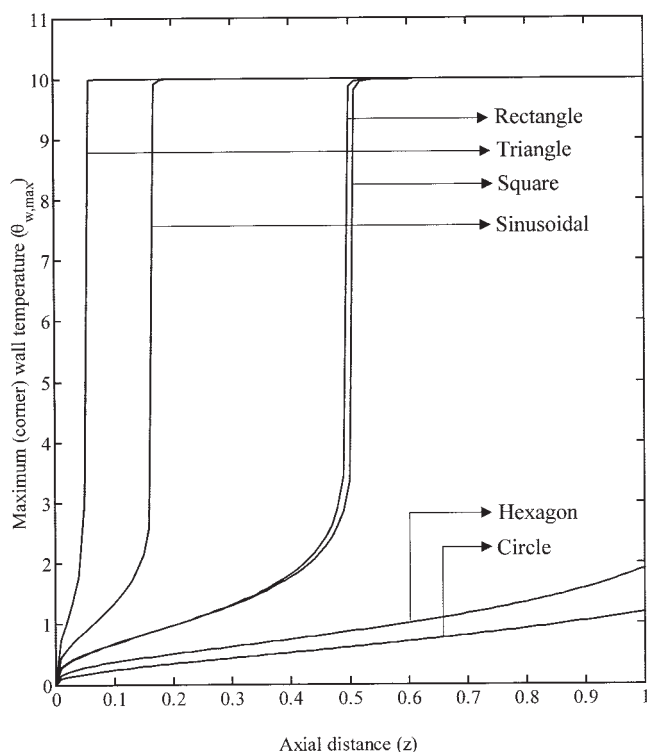


**Figure 14. Maximum (corner) surface/wall temperature along the axial distance obtained using the Convection model for different channel geometries for parameter values  $B = 10$ ,  $\phi_s^2 = 0.03$ ,  $\gamma = 25$ ,  $Le_f = 1$ ,  $P = 1$ ,  $\theta_{in} = 0$ ,  $\kappa = 0$ .**

It is not just sufficient for the monolith to be in the mass transfer controlled regime, but the exit cup-mixing conversion ( $\chi_m$ ) should also be sufficiently high, which depends on the mass transfer between the wall and the fluid. The exit cup-mixing concentration in the mass transfer controlled regime (for the Convection model) is given by Balakotaiah and West (2002)

$$c_m(z = 1) = 1 - \chi_m = \sum_{j=1}^{\infty} \alpha_j \exp\left(-\frac{\mu_j}{P}\right) \quad (49)$$

where  $\mu_j$  are the eigenvalues of the self-adjoint eigenvalue problem

$$\begin{aligned} \nabla^2 \psi &= -\mu_j f(x, y) \psi_j & \text{in } \Omega_1 \\ \psi_j &= 0 & \text{on } \partial\Omega_1 \end{aligned}$$

and the constants  $\alpha_j$  are given by the expression

$$\alpha_j = \frac{\langle 1, \psi_j \rangle^2}{\langle 1, \psi_j^2 \rangle}$$

where the inner product in the above equation is defined by

$$\langle \psi_i, \psi_j \rangle = \frac{\int_{\Omega_1} \psi_i(x, y) \psi_j(x, y) f(x, y) dA}{\int_{\Omega_1} f(x, y) dA}$$

These numerical constants  $\alpha_i$  and  $\mu_i$  ( $i = 1, 2, \dots$ ) determine the Sherwood number or the local mass transfer coefficient. A similar expression for conversion can also be derived for the case of the Short Monolith model. For the practical case of  $P < 1$ , one term is sufficient in the summation in Eq. 49 to predict the conversion to three decimal accuracy. Thus, for  $P < 1$

$$\chi_m \approx 1 - \alpha_1 \exp\left(-\frac{\mu_1}{P}\right) \quad (50)$$

One important point that should be noted here is that the  $P$  used in the above expressions is based on the ignited (mass transfer controlled) length of the channel and not the actual channel length. [Further details on the above expressions and detailed analysis can be found in Balakotaiah and West (2002) and Ramanathan et al. (2003).] The numerical constant  $\mu_1$  is related to the average asymptotic Sherwood number by

$$\mu_1 = \frac{Sh_T}{4} \quad (51)$$

Thus, to obtain high conversions in the mass transfer controlled regime, we not only need to have a larger ignited length

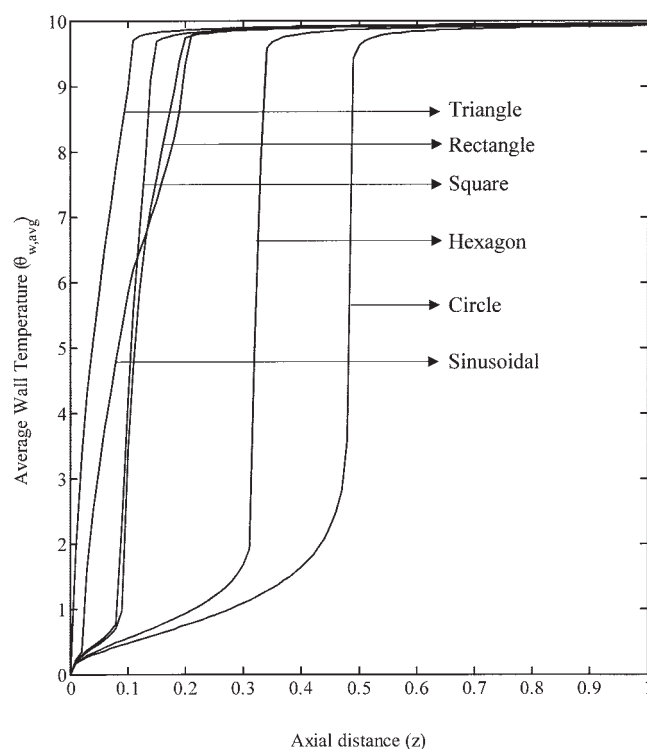


**Figure 15. Average surface/wall temperature along the axial distance obtained using the Convection model for different channel geometries for parameter values  $B = 10$ ,  $\phi_s^2 = 0.05$ ,  $\gamma = 25$ ,  $Le_f = 1$ ,  $P = 1$ ,  $\theta_{in} = 0$ ,  $\kappa = 0$ .**

(smaller effective  $P$  value) but also have a higher average mass transfer coefficient (higher value of  $Sh_T$ ). In Figure 15, the ignited length is almost double for triangular channels compared to that of circular channels, but the conversion is only slightly larger for triangular channels (55.5%) compared to that of circular channels (49.9%) because of the lower average mass transfer coefficient of triangular channels ( $Sh_T$  for a triangle is 2.497, whereas for a circle it is 3.656). To have a larger ignited length, the monolith should ignite earlier (or close to front-end ignition) and this would happen in geometries where the heat transfer coefficient is low (as explained earlier). For geometries having sharp corners, the low heat transfer coefficient near the corner helps to attain early ignition (and thus larger ignited length) but because of this low heat transfer coefficient near the corner, the average mass transfer coefficient becomes low and thus lowers the conversion. The heat/mass transfer coefficient has two contrasting effects, that is, low heat transfer coefficient helps in early ignition but high average mass transfer coefficient is required for higher conversions. To use the advantages of both the high and low heat/mass transfer coefficient effect, we can choose a geometry where the variation of the transfer coefficient along the channel perimeter is high with low transfer coefficient near the corner and much higher transfer coefficient along the sides so that the average transfer coefficient is high. This means that in Figure 2 we need to choose a geometry where the variation of the transfer coefficient along the channel perimeter is high and also the average transfer coefficient is high. Rectangular geometries with aspect ratio in the range 1:2 to 1:3 have both the corner effects (low transfer coefficients) and higher average transfer coefficient and thus give better conversion. For the simulations in Figure 15, the conversion is indeed best for the rectangular geometry (with aspect ratio 1:2).

The results discussed above are for the case of zero solid conduction. Peripheral solid conduction smooths out the variations of the wall temperature and thus as  $\kappa$  increases the wall temperature is almost uniform along the channel periphery. Figure 16 shows a plot of the average solid temperature profiles along the channel length for different values of  $\kappa$ . As can be seen, once the ratio  $\kappa$  becomes more than 10 the variation of the wall temperature along the channel periphery is substantially less. However, as shown in Figure 7,  $Nu_{avg}$  for  $\kappa = 10$  is closer to zero conduction limit in the entry region (before ignition). Although peripheral conduction leads to nearly uniform solid temperature across the channel (for  $\kappa \geq 10$ ) downstream of the ignition point, the local transfer coefficient ( $Nu_{loc}$ ) varies considerably across the channel in the upstream of the channel. Only in the limit of  $\kappa \rightarrow \infty$ , does the heat transfer coefficient become uniform across the channel both upstream and downstream of the ignition point. (As stated earlier  $\kappa$  has no influence on  $Sh_{loc}$ .) Thus, the corner effect is somewhat diminished and ignition is delayed for higher solid conductivities. Because the wall temperature is almost uniform for  $\kappa > 10$ , using the value of  $Nu_{H_1}$  in the ignition criterion (Eq. 45) is justified.

## Conclusions and Discussion

The main contribution of this work is the elucidation of the influence of channel geometry on ignition in catalytic monoliths. We have shown that in asymmetric geometries with sharp

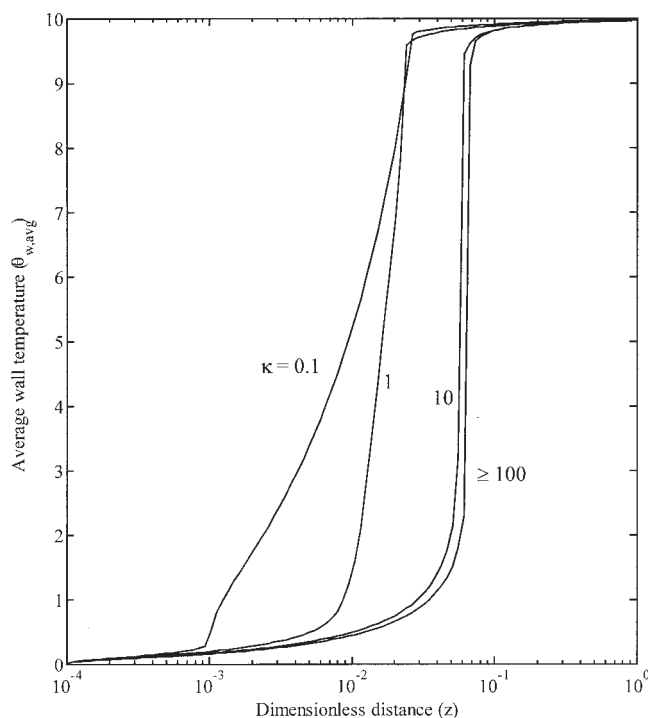


**Figure 16. Average surface/wall temperature along the axial distance obtained using the Convection model for triangular channels for different ratios of solid to fluid thermal conductivities.**

Parameter values  $B = 10$ ,  $\phi_s^2 = 0.1$ ,  $\gamma = 25$ ,  $Le_f = 1$ ,  $P = 1$ ,  $\theta_m = 0$ .

corners, ignition occurs first at the corners and spreads in the circumferential and axial directions. We have also shown that ignition depends strongly on the channel geometry when it occurs at the front end of the channel (that is, the second term of the ignition criterion exceeds unity). In practice, front-end ignition occurs when the catalyst loading or inlet temperature is high. Because this is common in many applications (such as catalytic combustion, automobile catalytic converters), the results of this study have practical relevance.

A second contribution of this work is the elucidation of the physical significance of the constant flux ( $Nu_{H_1}$  and  $Nu_{H_2}$  or  $Sh_{H_1}$  and  $Sh_{H_2}$ ) and constant wall temperature ( $Nu_T$  or  $Sh_T$ ) transfer coefficients in interpreting ignition in the 2-D (or 3-D) models and determining the conversion in the mass transfer controlled regime. Specifically, we have shown that  $Nu_{H_2}$  values correspond to local ignition (at corners), whereas  $Nu_{H_1}$  values correspond to ignition over the entire circumference of the channel. The difference between the numerical values of  $Nu_{H_2}$  and  $Nu_{H_1}$  is an indication of the nonuniformity of ignition in the circumferential direction. The value  $Sh_T$  (along with the Fourier weight  $\alpha_1$ ) determines conversion in the mass transfer controlled regime. This work also shows that high exit conversions are obtained in channel geometries that have high variation of the transfer coefficient along the channel perimeter (or lowest value for  $Nu_{H_2}$ ) and also having high average transfer coefficient (highest value for  $Sh_T$ ).

The results of this work may be combined with earlier results of Ramanathan et al. (2003) to determine the influence of peripheral as well as axial solid conduction on the light-off

boundary. The light-off criterion with solid conduction may be written as

$$\frac{g(\text{Pe}_h) B \phi_s^2}{P} + \frac{4e B \phi_s^2}{\text{Le}_f \text{Nu}(\kappa)} > 1 \quad (52a)$$

$$g(\text{Pe}_h) = \frac{1}{(\sigma_\theta^2 \sigma_\theta^2 / (1 - \sigma_\theta^2))} \quad \sigma_\theta^2 = \frac{2}{\text{Pe}_h} - \frac{2}{\text{Pe}_h^2} (1 - e^{-\text{Pe}_h}) \quad (52b)$$

$$\text{Pe}_h = \frac{\text{Pe}}{\delta \text{Le}_f \kappa} \quad (52c)$$

The function  $g(\text{Pe}_h)$  bounded between unity and  $e$  ( $=2.718$ ) accounts for the influence of axial conduction in the solid on the light-off boundary. The function  $\text{Nu}(\kappa)$  bounded between  $\text{Nu}_{H_2}$  and  $\text{Nu}_{H_1}$  accounts for the influence of peripheral solid conduction on the light-off boundary. Given that  $\text{Nu}_{H_1} \geq \text{Nu}_{H_2}$  (for all the geometries shown in Table 1), it may be concluded that peripheral solid conduction shrinks the region in which an ignited steady-state exists. In contrast, axial solid conduction expands this region. We also note that the influence of peripheral conduction on light-off region is much smaller compared to axial conduction. [The ratio  $\text{Nu}_{H_1}/\text{Nu}_{H_2}$  varies from 1 to 1.643 for the geometries shown in Table 1, whereas  $g(\text{Pe}_h)$  varies from unity (at  $\text{Pe}_h = \infty$  or  $\kappa = 0$ ) to 2.718 (at  $\text{Pe}_h = 0$  or  $\kappa = \infty$ ).]

For simplicity, we have assumed in this work that the washcoat is very thin and considered only the wall reaction case. In practice, the washcoat thickness is finite and more catalyst/washcoat tends to accumulate near the corners as a result of surface tension effects. (Typical channel transverse dimension may be  $500 \mu\text{m}$ , whereas the washcoat thickness varies from around  $10 \mu\text{m}$  on the sides to around  $50 \mu\text{m}$  at the corners.) Thus, the corners are not as sharp when the washcoat is added and this is expected to diminish the corner effect on ignition. However, this may be partially compensated by the fact that there is more catalyst now at the corner (leading to a higher effective rate constant), which enhances the likelihood of ignition. A complete understanding of the ignition phenomenon in washcoated monoliths requires the solution of the convective–diffusion equations in the channel geometry coupled to diffusion–reaction equations in the washcoat.

Finally, this work examined the effect of geometry on ignition for internal duct flows. The nonuniform ignition found here is also present in external flows (such as flow around a spherical catalyst particle or cylindrical wire, etc.), where the nonuniform flow field leads to the variation of the transfer coefficient on the surface. The variation of the Sherwood/Nusselt number in such 3-D flows is typically much higher than that examined here. For example, even for flow around smooth objects, such as a sphere or cylindrical wire, the ratio of  $\text{Nu}_{\max}/\text{Nu}_{\min}$  is around 8. This ratio is expected to be even higher for objects with sharp edges or corners (such as finite cylinders). In such cases, ignition is expected to occur (for the case of an exothermic reaction with monotone kinetics) at points where the Nusselt number is a minimum and spread over the rest of the object. Understanding of such nonuniform ignition (or extinction) is important in determining the true kinetic or transport parameters from single pellet/particle experiments.

## Notation

$A_\Omega$	= channel cross-sectional area
$B$	= dimensionless adiabatic temperature increase
$c$	= dimensionless concentration
$c_{pf}$	= fluid specific heat capacity
$C$	= concentration
$C_o$	= inlet fluid concentration
$d_h$	= channel hydraulic diameter
$D_m$	= diffusion coefficient in the fluid phase
$\text{Da}$	= monolith Damköhler number
$E$	= activation energy
$f(x, y)$	= dimensionless velocity profile
$h$	= heat transfer coefficient
$k_f$	= fluid thermal conductivity
$k_c$	= mass transfer coefficient
$k_s$	= solid thermal conductivity
$k_w$	= effective rate constant for surface (wall) reaction
$L$	= length of the monolith channel
$\text{Le}_f$	= fluid Lewis number
$\text{Nu}$	= Nusselt number
$P$	= transverse Peclet number
$P_\Omega$	= perimeter of channel
$\text{Pe}$	= axial Peclet number
$R_g$	= universal gas constant
$R_\Omega$	= one-half the channel hydraulic radius
$\text{Sh}$	= Sherwood number
$T$	= fluid temperature
$T_o$	= inlet fluid temperature
$\langle u \rangle$	= average fluid velocity
$x, y$	= transverse coordinate (dimensionless)
$z$	= coordinate along the length of the channel (dimensionless)

## Greek letters

$\alpha$	= monolith aspect ratio ( $4R_\Omega/L$ )
$\gamma$	= dimensionless activation energy
$\kappa$	= ratio of solid to fluid thermal conductivity
$\rho_f$	= fluid density
$\phi_s$	= Thiele modulus (local Damköhler number)
$\theta$	= dimensionless temperature
$\chi_m$	= exit conversion

## Subscripts and superscripts

'	= dimensional
avg	= average
loc	= local
m	= mixing-cup
s	= solid
w	= wall

## Acknowledgments

This work was supported by grants from the Robert A. Welch Foundation, Texas Advanced Technology Program, and The Dow Chemical Company.

## Literature Cited

- Balakotaiah, V., N. Gupta, and D. H. West, "A Simplified Model for Analyzing Catalytic Reactions in Short Monoliths," *Chem. Eng. Sci.*, **55**, 5367 (2000).
- Balakotaiah, V., and D. H. West, "Shape Normalization and Analysis of the Mass Transfer Controlled Regime in Catalytic Monoliths," *Chem. Eng. Sci.*, **57**, 1269 (2002).
- Benedetto, A. D., A. S. Marra, and G. Russo, "Heat and Mass Fluxes in Presence of Superficial Reaction in a Not Completely Developed Laminar Flow," *Chem. Eng. Sci.*, **58**, 1079 (2003).
- Damköhler, G., "Influence of Diffusion, Fluid Flow and Heat Transfer on the Yield in Chemical Reactors," *Chem.-Ing.-Tech.*, **3**, 359 (1937).
- Groppi, G., A. Belloli, E. Tronconi, and P. Forzatti, "A Comparison of

- Lumped and Distributed Models of Monolith Catalytic Combustors," *Chem. Eng. Sci.*, **50**, 2705 (1995a).
- Groppi, G., A. Belloli, E. Tronconi, and P. Forzatti, "Analysis of Multi-dimensional Models of Monolith Catalysts for Hybrid Combustors," *AIChE J.*, **41**, 2250 (1995b).
- Groppi, G., and E. Tronconi, "Theoretical Analysis of Mass and Heat Transfer in Monolith Catalysts with Triangular Channels," *Chem. Eng. Sci.*, **52**, 3521 (1997).
- Groppi, G., E. Tronconi, M. Berg, and P. Forzatti, "Development and Application of Mathematical Models of Pilot-Scale Catalytic Combustors Fueled by Gasified Biomasses," *Ind. Eng. Chem. Res.*, **39**, 4106 (2000).
- Gupta, N., and V. Balakotaiah, "Heat and Mass Transfer Coefficients in Catalytic Monoliths," *Chem. Eng. Sci.*, **56**, 4771 (2001).
- Hayes, R. E., and S. T. Kolaczowski, "Mass and Heat Transfer Effects in Catalytic Monolith Reactors," *Chem. Eng. Sci.*, **49**, 3587 (1994).
- Hayes, R. E., S. T. Kolaczowski, J. Thomas, and J. Titiloye, "Transient Experiments and Modeling of the Catalytic Combustion of Methane in a Monolith Reactor," *Ind. Eng. Chem. Res.*, **35**, 406 (1996).
- Heck, R. H., J. Wei, and J. R. Katzer, "Mathematical Modeling of Monolithic Catalysts," *AIChE J.*, **22**, 477 (1976).
- Ramanathan, K., V. Balakotaiah, and D. H. West, "Light-Off Criterion and Transient Analysis of Catalytic Monoliths," *Chem. Eng. Sci.*, **58**, 1381 (2003).
- Shah, R. K., and A. London, *Laminar Forced Convection in Ducts*, Academic Press, New York (1978).
- Tronci, S., R. Baratti, and A. Gavrilidis, "Catalytic Converter Design for Minimisation of Coldstart Emissions," *Chem. Eng. Commun.*, **173**, 53 (1999).
- Tronconi, E., and P. Forzatti, "Adequacy of Lumped Parameter Models for SCR Reactors with Monolith Structure," *AIChE J.*, **38**, 201 (1992).
- Young, L. C., and B. A. Finlayson, "Mathematical Models of Monolith Catalytic Convertors," *AIChE J.*, **22**, 331 (1976).

*Manuscript received June 26, 2003, and revision received Aug. 22, 2003.*